

Tracer Studies in a Laboratory Beach Subjected to Waves

Michel C. Boufadel¹; Hailong Li²; Makram T. Suidan³; and Albert D. Venosa⁴

Abstract: This work investigated the washout of dissolved nutrients from beaches due to waves by conducting tracer studies in a laboratory beach facility. The effects of waves were studied in the case where the beach was subjected to the tide, and that in which no tidal action was present. The following may be inferred: (1) waves created a steep hydraulic gradient in the swash zone and a mild one landward of it; (2) waves increased the residence time of a plume when they broke seaward of it. They also created additional pathways for transport of the tracer to the beach surface; and (3) in the presence of a tide that completely covered the solute plume, overall, the waves increased the washout of the tracer from the intertidal zone of the beach in comparison with the no-wave case. The residence time of the tracer plume due to waves superimposed on the tide was estimated as 75% of that resulting from the tide with no waves. Discussion on scaling up the results and implications for bioremediation are also presented.

DOI: 10.1061/(ASCE)0733-9372(2007)133:7(722)

CE Database subject headings: Waves; Tides; Beaches; Tracers; Nutrients; Laboratory tests; Biological treatment.

Introduction

Understanding the effects of waves on water flow and solute transport in beaches is important in many applications such as bioremediation of oil spills on beaches and the transport of contaminants to sea. Most existing works on waves considered the effects of waves in the context of preventing damages resulting from large waves, such as a tsunami (Spielvogel 1975). In such cases, the beach was considered impermeable and focus was directed to predicting the wave runup (Gourlay 1992). Few studies investigated the effects of waves on beach hydraulics. Riedl et al. (1972) and Riedl and Machan (1972) found that waves result in a “pumping” mechanism whereby water is exchanged between the beach and the sea. More recent studies (Nielsen 1989; Hegge and Masselink 1991; Asservatham et al. 1993) found that waves result in two zones in the beach have different hydraulic gradients: A zone landward of the swash zone with a mild seaward hydraulic gradient and the swash zone with a much steeper gradient.

This paper reinvestigates the presence of two gradients, and focuses on the solute transport in the beach. This is done by conducting tracer studies in a laboratory beach facility using sodium chloride (NaCl), a conservative tracer, and monitoring its movement using electrical conductivity meters. This paper starts with definitions and concepts related to waves taken from the

coastal engineering terminology. Next, an explanation on how the tide is generated is reported, followed by a description of the wavemaker and how to generate waves of (relatively) constant height. Water-only experiments (i.e., no tracer) are then reported to investigate the effects of waves on the water table. These are followed by experiments of tracer transport in the beach due to waves in the absence of tides. Finally, experiments of tracer transport due to waves superimposed on the tide are reported. These are compared to experiments of a previous work (Boufadel et al. 2006) where the transport was due to the tide only (i.e., in the absence of waves).

Concepts and Definitions

The most important parameters to describe a wave are its length, L , and height, H , and the water depth, h , over which it is propagating (Dean and Dalrymple 1984). The length of a wave, L , is the distance between two consecutive crests or troughs; the wave height, H , is the vertical distance between crest and trough; and the water depth, h , is the average vertical distance of the wave crest and trough to the bottom. One also defines the mean water level (MWL) which, as the name indicates, is the average water level at sea. The still water level (SWL) is a horizontal line representing the sea state in the absence of the waves. The MWL is identical to the SWL far offshore, but varies as the waves approach the shore (discussed below).

An important parameter that emerges is the relative depth h/L (Dean and Dalrymple 1984). For $h/L > 0.5$, deep water conditions reign where the wave does not “feel” the bottom. For $h/L < 0.05$ shallow water conditions prevail and the bottom affects the wave characteristics causing the horizontal water velocity to be essentially uniform with the depth. In such a case, the wave behaves as a hydraulic bore. Note that these definitions are rather qualitative because the change in the wave characteristics is gradual for a gradual variation in the depth.

In deep water (i.e., $h/L > 0.5$), the first order theory (also known as the linear theory) indicates that the wave length L is related to the wave period T by the equation

¹Associate Professor, Dept. of Civil and Environmental Engineering, Temple Univ., Philadelphia, PA, 19122. E-mail: boufadel@temple.edu

²Postdoctoral Fellow, Dept. of Civil and Environmental Engineering, Temple Univ., Philadelphia, PA, 19122. E-mail: hailong@graduate.hku.hk

³Herman Schneider Professor, Dept. of Civil and Environmental Engineering, Univ. of Cincinnati, Cincinnati, OH.

⁴Microbiologist, U.S. Environmental Protection Agency, National Risk Management Research Laboratory, Cincinnati, OH.

Note. Discussion open until December 1, 2007. Separate discussions must be submitted for individual papers. To extend the closing date by one month, a written request must be filed with the ASCE Managing Editor. The manuscript for this paper was submitted for review and possible publication on August 10, 2006; approved on November 16, 2006. This paper is part of the *Journal of Environmental Engineering*, Vol. 133, No. 7, July 1, 2007. ©ASCE, ISSN 0733-9372/2007/7-722-732/\$25.00.

$$L = \frac{g}{2\pi} T^2 \quad (1)$$

where $g[LT^{-2}]$ =gravity acceleration. Another equation of interest is that giving the speed of propagation of the wave, C

$$C = \frac{L}{T} = \frac{g}{2\pi} T \quad (2)$$

The first equality in Eq. (2) is the definition of wave speed (wavelength over wave period), and the second equality results from Eq. (1). Eq. (1) indicates that the wave speed is proportional to the wave period. This means that waves of large periods propagate faster than those of small periods. Based on Eq. (2), this also means that long waves propagate faster than short waves. For this reason, Eq. (1) is commonly known in the ocean engineering literature as the “wave dispersion equation”, because it describes how waves of various periods move at various speeds and, thus, “disperse” (i.e., move away) from each other.

Several changes occur as a wave shoals (i.e., propagates into shallow water). One of the most obvious is the increase in wave height. However, the wave height cannot increase indefinitely; at some depth, the wave becomes hydrodynamically unstable and breaks. The maximum wave uprush defines the wave runup, while the lowest backwash is the rundown. These limits are commonly measured as distances (along the beach surface) from the intersection of the SWL and the beach surface. The zone between the rundown and the runup is the swash zone.

The MWL varies as the waves approach the shore. Due to exchange of momentum resulting from the so called radiation stress (Longuet-Higgins and Stewart 1964), the MWL could be lower than the SWL. This is known as setdown. However, in the swash zone, the MWL is higher than the SWL and is commonly referred to as wave setup. In addition, the mean water table is commonly above the SWL, and thus, the setup is considered to extend into the porous sediments. More information on basic wave hydrodynamics can be found in the works by Dean and Dalrymple (1984).

Beach Mesocosm

Experimental Layout

The facility used in the experiment consisted of an 8 m long \times 2 m high \times 0.6 m wide carbon steel tank as depicted schematically in Fig. 1. One of the long vertical sides (8 \times 2 m) was made transparent using plexiglass sheets. The sand was positioned at a slope of 10% from a height of 115–65 cm and at 40% slope from 65 cm to zero, which results in a total horizontal sand coverage of about 630 cm. A screen made of expanded steel and fine mesh was installed 30 cm from the landward wall (Fig. 1) to hold the sand and to allow water passage. In Fig. 1, the water volume landward of the screen represented the landward water table, while the open water volume seaward of the beach represented the sea. Two “sacrificial” zinc plates were placed in the tank on both ends to reduce steel corrosion from the tank. Zinc was selected because it has a higher oxidation potential than steel.

Sand Properties

The sand used in the tank was coarse with a median size of 1.0 mm and a narrow particle size distribution, varying from 0.8 and 1.2 mm. Due to the coarseness of the sand, little transport

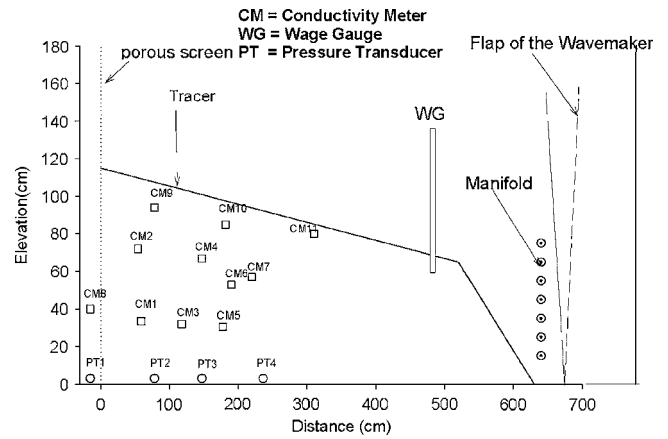


Fig. 1. Experimental beach setup and the wavemaker. The locations of the sensors are also shown.

of sand by suspension is expected to occur. Before the sand was placed in the tank, its porosity was measured by filling a 4 L beaker with well drained sand and adding a sufficient amount of water to produce ponding conditions at the sand surface. The ratio of the volume of the added water to the bulk volume of the sand (solid+voids) is, by definition, the porosity of the medium (Freeze and Cherry 1979). This porosity value was 0.38. The sand was compacted in place using a concrete vibrator to eliminate water channeling. The porosity of the sand in the tank was estimated in situ by observing the settlement of the beach sand profile after compaction. The reduction in sand height in the beach was about 13% resulting in a porosity of $0.38(1.0-0.13)=0.33$. The saturated hydraulic conductivity of the compacted sand was estimated in Boufadel et al. (1998) using both the Kozeny formula (Bear 1988) and calibration of the subsurface flow model MARUN (Boufadel et al. 1999). This gave the value 0.2 cm/s. The van Genuchten (1980) unsaturated parameters of the sand were estimated by the calibration in Boufadel et al. (1998), who found $\alpha=0.155 \text{ cm}^{-1}$ and $n=3.5$. The inverse of α (equal to 6.45 cm herein) provides an estimate of the capillary fringe (zone of considerable moisture above the water table). The parameter n represents the pore size distribution, and higher n values imply more uniform distributions. The estimated value of n falls on the high end of typical n values in natural systems, which range from 1.2–3.0 (Morell-Seytoux et al. 1996). This is expected due to the narrow grain size distribution of the sand. More information on the parameters α and n can be found elsewhere (van Genuchten 1980; Boufadel et al. 1998, 1999; Naba et al. 2002).

Sensors

The experiments required the measurements of the water levels and the concentration of salt. The open water level on the sea side of the tank was measured using a wave gauge (WG, Model No. LV5900, Omega Engineering) with an accuracy of 1.0 mm. The readings of the WG were logged using a Strawberry Tree data software (Strawberry Software, Inc., California). Four pressure transducers (PT, Model No. 1151AP, Fisher) placed at the bottom of the tank measured the water level behind the screen and in the beach. The PTs were accurate to 1.0 mm, and their readings were also logged by the Strawberry Tree data software. In addition, the software was used to control the water level in the tank

Table 1. Locations of Pressure, Water Level, and Concentration Sensors

Sensor	x (cm)	z (cm)	y (cm)
PT1 ^a	-15	3	60
PT2	78	3	60
PT3	147	3	60
PT4	235.5	3	60
WG	520	NA ^b	30
CM1	59	33.5	20
CM2	54.5	72	45
CM3	118	32	40
CM4	147	67	15
CM5	177	30.5	50
CM6	190	53	30
CM7	220	57	50
CM8 ^a	-15	40	30
CM9	78	94	15
CM10	181	85	10
CM11	310	80	20

Note: x =horizontal distance from the screen (positive seaward); z =elevation from the bottom of the tank; y =horizontal depth from the plexiglass wall (positive inward perpendicular to the plan of Fig. 2).

^aThe sensor is landward of the screen.

^bNA: Not applicable.

by sending the appropriate electronic signal to the inflow and the outflow pumps. The locations of the water level devices are given in Table 1 and shown in Fig. 1.

The concentration of the salt was measured by conductivity meters (CM, CDCN 108, Omega Engineering). The readings of the CM's were logged to a data logger of type CR10 (Rocktest, Inc., Plattsburg, New York). The accuracy in the CMs readings was around 95%, always larger than 90% (i.e., the error is less than 10% of the reading). The CMs were in the shape of a hollow disk (doughnut) with dimensions of $10 \times 2.5 \times 3$ cm representing the exterior diameter, the interior diameter, and the thickness, respectively. Early experimentation with the sensors showed that they were not reliable when they were in contact with the sand. For this reason, each CM was placed in a special casing made of plexiglass. The casings were slotted on all sides and covered with a stainless mesh of hole size about 0.1 mm.

The locations of the probes along the length of the tank are listed in Table 1 and shown in Fig. 1. The horizontal distances of the CMs from the plexiglass wall were different to minimize the sensor interactions along the general flow direction (landward-seaward).

Tide Simulation

The tide was simulated by pumping water in and out of the tank periodically. Because the tide can be viewed as a shallow wave, the horizontal velocity of the water is approximately uniform with the depth (Dean and Dalrymple 1984). This was simulated with two manifolds that were placed vertically on each of the long sides of the tank (Fig. 1). The flow of water in and out of the tank was through the manifolds, and it was driven by two pumps and one three-way solenoid valve. The water exiting the wave tank was wasted to the drain.

The height of the simulated tide varied between 70 and 110 cm with a tidal period of about 37.5 min. This period was chosen based on the pumps capabilities, and Boufadel et al.

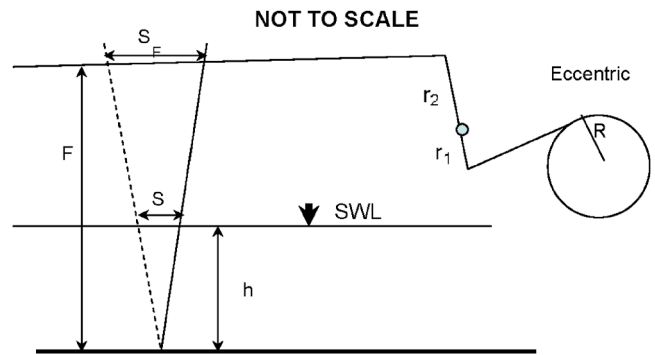


Fig. 2. Variable lever mechanism to adjust the wave height for a variable SWL

(2006) showed that this period could be scaled up to represent a semidiurnal tidal period. Because the beach slope in the intertidal zone was 10%, the length of the intertidal zone was 400 cm. The high tide and low tide lines (the tide line is the intersection of the sea water level and the beach surface) were at 50 and 450 cm from the screen.

Wavemaker

The wavelength was designed to be less than 2.5 m to reduce reflection from the beach. This is because long waves have higher reflection than shorter waves (Ippen 1966). For the intermediate tide value of 90 cm, the ratio h/L computed near the wavemaker is 0.36, which is close to the deep water limit of 0.5. Using particle imaging, Melville et al. (2002) observed that a value of 0.3 still provides essentially deep-wave behavior. This means that waves in the tank are almost deep-water waves, which would be better generated by a flap-type wavemaker instead of a piston-type wavemaker. This is because the kinematics of the waves generated with the piston resembles more closely a water bore where the horizontal water velocity is uniform with the depth (Svendsen 1985).

Wave generation was obtained as the result of the rotation of an eccentric flywheel. The flywheel was connected from one end to a motor and from the other to the flap via an actuator shaft as seen in Fig. 2. The flywheel was driven through a gear by a five horse-power (3.75 kW) motor. The motor runs at a constant speed, thus, producing a sinusoidal in time actuator motion of period T , where T is the period of the design wave. This provides a sinusoidal flap motion with the maximum displacement S_F located at the connection with the actuator. As seen in Fig. 2, S_F is twice the radius R of the eccentric wheel. The stroke, S , at the SWL is given by the triangle relation

$$S = \frac{h}{F} S_F \quad (3)$$

Experimentation with the system revealed that the generated wave increased in height as the SWL was increased. This was due to the fact that the flap is hinged at the bottom, and increase in the SWL results in an increase in S , as given by Eq. (3). To generate a wave with a height that does not change with the tide, a system was built to reduce the S_F as the h increased. This was implemented by changing r_2 with the tide, as discussed next. For a constant horizontal displacement $2R$ (where R is the radius of the eccentric wheel) of the actuator, the lever mechanism provided a horizontal displacement S_F given by

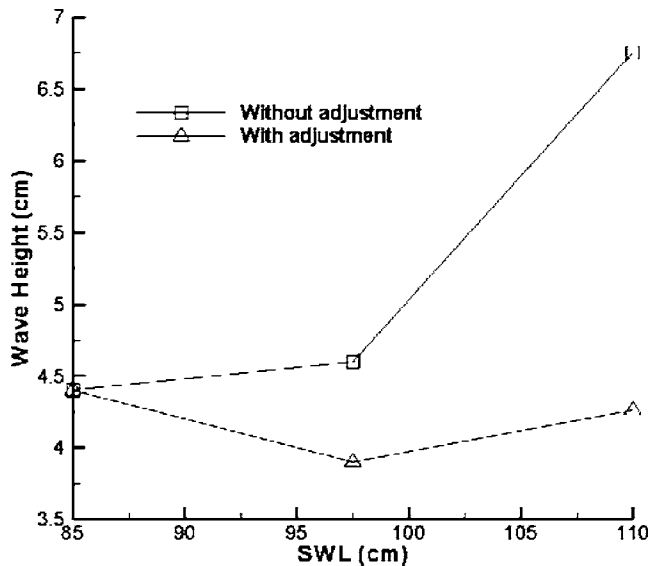


Fig. 3. Quasi-constancy of wave height as the SWL varies thanks to the continuous adjustment of the stroke of the flap (by varying r_2 , Fig. 2), $T=1.25$ s

$$S_F = \frac{r_2}{r_1}(2R) \quad (4)$$

where r_1 and r_2 are given in Fig. 2. The distance r_1 was set constant, while r_2 was allowed to vary from 2.0–10.0 cm using a slide that moved along two 3/8 in. steel shafts, and powered by a 1/2 horsepower (375 Watt) motor (Bodine, Chicago, Ill.). The connection between the slide and the motor was via a lovejoy connection. The stroke adjustment was controlled by the computer as follows: At low tide, the value of r_2 was set at its maximum. When the water level increased, a sensor sent a signal to the computer, which in turn sent a signal to the motor controlling the slide informing it to decrease the variable arm r_2 of the lever by a certain amount obtained from a calibration curve. This resulted in a reduction in S_F at the new SWL, and the procedure was repeated until the SWL reaches the maximum value (i.e., the high tide), where the procedure was reversed.

Experiments were conducted to assess the effects of the stroke adjustment on the wave height. The wave period was 1.25 s and 3 SWL were considered: 85.0, 97.5, and 110 cm. Fig. 3 shows that when no adjustment was made, the wave height increased continuously with the SWL. However, the adjustment through the lever mechanism provided an essentially constant wave height.

Experiments

Effect of Waves on Beach Water Table

The goal of these experiments was to assess the rise of the beach water table due to the waves. The experiments were performed by achieving, first, a hydrostatic equilibrium of the water throughout the tank, and then starting the wavemaker. No water was added to or withdrawn from the tank during the experiments. Two still water levels, SWL, (80 and 90 cm) and three wave periods (1.0, 1.11, and 1.25 s) were considered resulting in six experiments. The 80 cm SWL intersected the beach at $x=350$ cm, and the 90 cm SWL intersected the beach at $x=250$ cm.

Table 2. Properties of Waves at Two Still Water Levels and Effect on Beach Water Table

T (s)	SWL=80 cm		SWL=90 cm	
	H (cm)	RWT (cm)	H (cm)	RWT (cm)
1.00	4.5	0.9	5.4	2.0
1.11	4.0	1.9	4.8	2.2
1.25	2.5	2.1	4.5	1.6

Note: H =wave height (vertical distance between trough and crest); and RWT=rise of water level at PT1 (Fig. 1 and Table 1) from initial SWL.

At each SWL, the wave height decreased with an increase in the wave period, as reported in Table 2. This is to be expected, because the constancy of the stroke at a given SWL results in constancy of the water volume being pushed. Because larger wave periods result in larger wave lengths [Eq. (1) or (2)], the height of the wave has to decrease to satisfy the mass conservation. In all the experiments, a sand bar formed in the swash zone in about 10 min. Detailed measurements of the profile and the location of the sand bars were not made. The runup at the beginning of experiments were (approximately) 20, 40, and 50 cm for wave periods $T=1.0$, 1.11, and 1.25 s, respectively, as observed through the transparent side of the tank. Even after the formation of the sand bars, waves with larger periods continued to have larger runups.

Figs. 4 and 5 show the variation of the water level at the PTs (Fig. 1 and Table 1) as a function of time for SWL 80 and 90 cm, respectively. All the PTs indicate a rise in the (beach) water table with time. The WG indicated that the MWL decreased with time, which is due simply to the fact that the volume of open water decreased as it filled the beach. Fig. 4 shows that the rise of the PTs in response to waves was concordant with their landward placement with respect to the swash zone; the most seaward PT rose first, followed by the second most seaward PT, etc. This configuration, which indicates a landward hydraulic gradient, remained the same for about 30 min. The relatively sudden decrease in the water level in Fig. 4(b) at $t=25$ min was probably due to partial removal of the sand bar, which held water landward of it. For each experiment, the water level reached essentially the same value at all sensors indicating that the hydraulic gradient landward of the swash zone is essentially zero (i.e., a horizontal water table). The final elevation of the water table (say for $t>50$ min) seems to increase with the wave period, especially when comparing Fig. 4(a) ($T=1.0$ s) to Figs. 4(b and c) ($T=1.11$ and 1.25 s, respectively). This is understandable, because the runup is the primary mechanism that fills the beach for such high hydraulic conductivity sediments (Gourlay 1992; Asservatham et al. 1993). Note that the runup increased with the wave period.

For SWL=90 cm (Fig. 5), the three most seaward sensors (PT4, PT3, and PT2) rose essentially at the same time, and were lagged by PT1. Their rise was faster than in Fig. 4, because the sensors are closer to the swash zone for this SWL. For times greater than 30 min, the three most landward sensors reached the same value, but the pressure at PT4 remained about 1.0 cm lower. This indicates that the hydraulic gradient between PT4 and PT3 is steeper than that landward of PT3. Noting that PT4 is in the swash zone, one concludes that two hydraulic gradients exist in the beach; a mild (near zero) hydraulic gradient landward of the swash zone, and a steep (seaward) hydraulic gradient in the swash zone. This is in agreement with previous studies (Nielsen 1989;

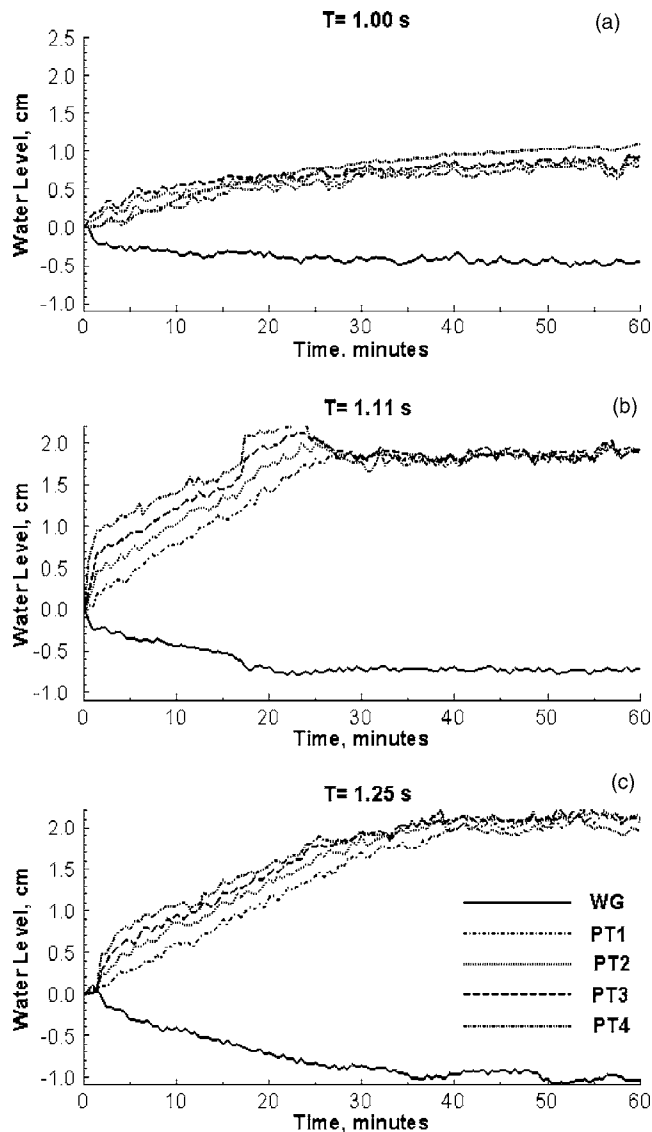


Fig. 4. Variation of the mean water level and the water table due to waves for an initial SWL=80 cm and three wave periods: (a) $T=1.25$ s; (b) $T=1.11$ s; and (c) $T=1.0$ s. The value 0.0 on the vertical axis represents 80 cm. All PTs were landward of the swash zone, and they indicate that the elevation of water table above them increased with time.

Hegge and Masselink 1991; Asservatham et al. 1993). The final rise of the water table did not appear to increase with the wave period, most likely due to the continuously varying profile in the swash zone; for $T=1.25$ s, it is most probable that a small sand bar formed and reduced the runup. Note that the rise of the water table suddenly increased at $t=60$ min, most likely due to the clearing of the sand bar by waves. An empirical relation that predicts the increase of the setup landward of the swash zone as a function of the runup was proposed by Asservatham et al. (1993). Such a relation will not be verified herein, because it requires measurements that were not taken in this work.

Tracer Movement due to Waves without Tide

The use of a tracer in these experiments, which is not commonly done in the coastal engineering community, provided a means for

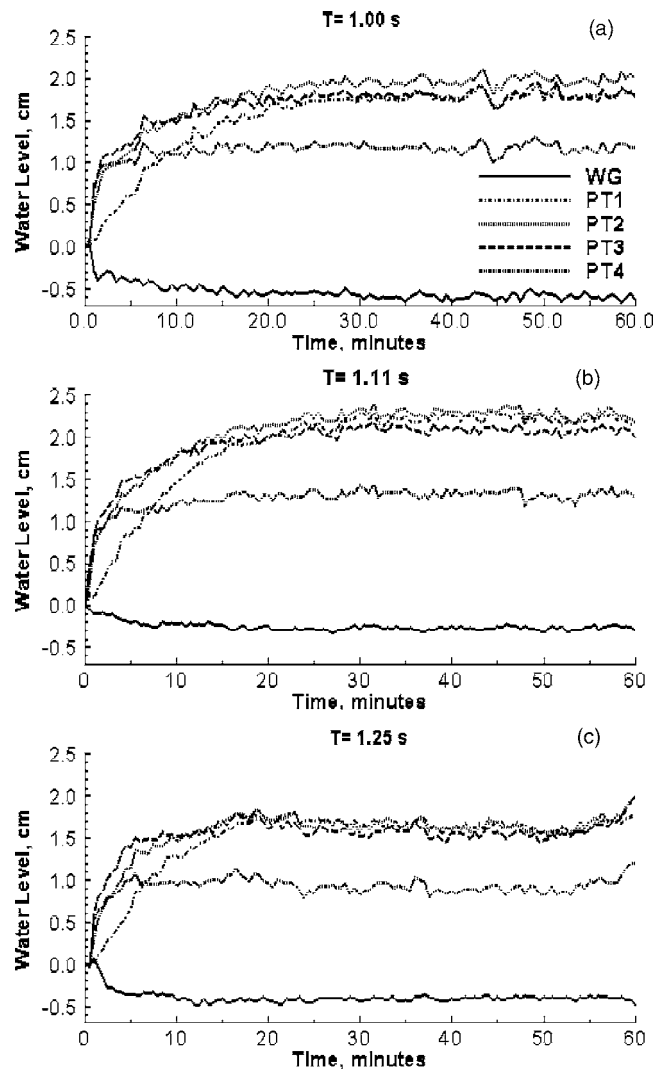


Fig. 5. Variation of the mean water level and the water table for an initial SWL=90 cm and three wave periods: (a) $T=1.25$ s; (b) $T=1.11$ s; and (c) $T=1.0$ s. The value 0.0 on the vertical axis represents 90 cm. PT4 was in the swash zone and did not increase as much as the remaining PTs.

understanding the transport and hydrodynamics at many locations in the beach, rather than focusing solely on the water table motion.

The water level landward of the beach (PT1) was fixed at 100 cm and the water level in the sea (at WG) was fixed at 90 cm. The water level at PT1 was controlled by the computer, which controlled an inlet pump to introduce water landward of the screen whenever the reading at PT1 dropped 0.3 cm below 100 cm. A similar control took place at the sea side; the outflow pump was turned on whenever the reading at the wave gauge increased 0.3 cm above 90 cm. The outflow from the tank was wasted to the drain. To control the SWL movement in the presence of the waves, readings from WG (Fig. 1) were taken every 0.1 s, averaged over 120 s, and then reported to the controlling software every 30 s. The remaining water pressure/level and concentration data were taken and logged every 30 s. This method of data logging/system control was used whenever waves were present.

One experiment was conducted when no waves were present and duplicate experiments were conducted for the wave case

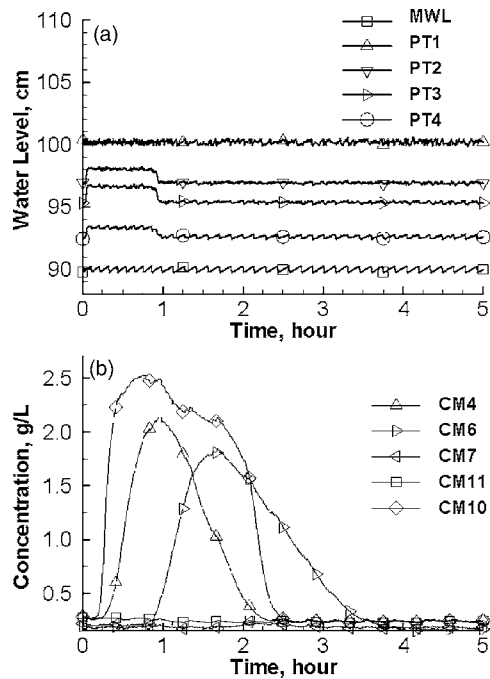


Fig. 6. Seaward gradient for the no-wave cases observed: (a) water levels; (b) concentrations

($T=1.11$ s). However, only one of the duplicate wave experiments is reported here for brevity. The other experiment can be found in the work of Boufadel (1998). In both the wave and the no-wave cases, the experiments started by achieving a steady state hydraulic regime by fixing the water levels as mentioned above. Then, 100 L of NaCl solution at 2.76 g/L were applied onto the beach surface at $x=126$ cm (and $z=103$ cm), see Fig. 1. An one-half inch perforated manifold was used to spread the solution across the width of the tank. The application of the tracer took 50–55 min in each of three experiments that were conducted. Very little ponding occurred on the beach surface due to the high hydraulic conductivity of the beach sand (see the section on the sand above). No other action was taken for the no-wave case. For the wave case, the wavemaker was started immediately after the tracer application. The wave height was about 4 cm in deep water. The runup decreased from about 40 cm at the beginning of the experiment to about 15 cm at the end of the experiments. The rundown was about 5 cm. The reduction in the runup length was due to the formation of a sand bar around $x=235$ cm, which is landward of the intersection point of the beach water table with the SWL ($x=250$ cm, $z=90$ cm), thereby, blocking the landward water excursion. CM11 was used ($x=310$ cm, $z=80$ cm) and CM9 was not used.

The results of the no-wave control are shown in Fig. 6. The application of the tracer caused a sudden increase in the beach water table [Fig. 6(a)], but did not reverse the seaward hydraulic gradient, because the water level in the beach remained below that of PT1. Fig. 6(b) shows that the concentration at CM10 rose first reaching the maximum, and remained relatively high for a duration of approximately 2 h. The concentration at CM4 increased next reaching about 90% of the maximum. It decreased sharply afterwards. The concentration at CM6 increased at a much latter time compared to the other sensors.

The waves (Fig. 7) did not seem to affect much the rise time (or rise to peak) at the sensors CM4, CM6, and CM10, but they increased the “width” of the breakthrough curves at all concen-

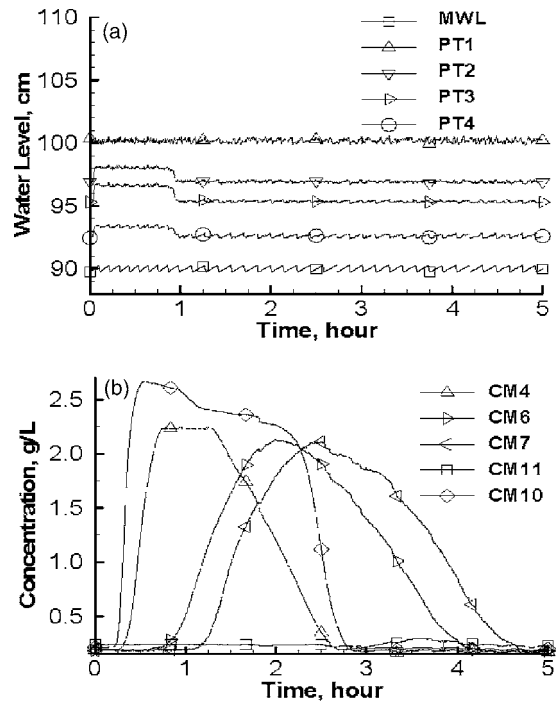


Fig. 7. Seaward gradient for the cases with waves observed: (a) water levels; (b) concentrations. The waves had a period $T=1.11$ s. The plume stayed longer in the beach in comparison to the no-wave case (Fig. 6).

tration values. For example, if one considers only the “base-time” (the period between the two zero crossings) of CM6, it starts at the same time for both cases and ends at 3.5 and 4 h for the no-wave and wave cases, respectively. Hence, the increase is 20%. This implies that the residence time at this sensor is increased by more than 20%. This is because the width of the breakthrough curve increased (due to waves) at all concentration values and not only at the base.

Waves appeared to have affected not only the residence time of the plume, but also its pathways; the concentration at CM7 reached approximately 80% of the maximum for the wave case [Fig. 7(b)], while it remained at background for the no-wave case [Fig. 6(b)]. This indicates that waves created a new pathway in the beach, through CM7 (Fig. 1), that carried the plume closer to the beach surface (in particular the swash zone). One could understand the increase in the residence due to the “flattening” of the water table as noted from the previous section, but this new pathway deserves more attention. As an indication, note the slight increase in concentration at CM11 in Fig. 7(b) (at $t=3.5$ h) in comparison to Fig. 6(b). This suggests that a mechanism in the swash zone caused the plume to move more horizontally than in the no-wave case. We believe that after the plume reached below the swash zone, the waves during runup were engulfing small areas of the plume and entraining them to sea during rundown. It is also possible that the rundown created suction on the beach surface that “drew” the water (and the dissolved plume) closer to the surface. These are the only explanations that we could give at this juncture. We will investigate them in future works. It is worth noting that the three experiments were conducted within a week, with the no-wave experiment in the middle. Thus, we believe that a malfunction of the sensor CM7 should be ruled out.

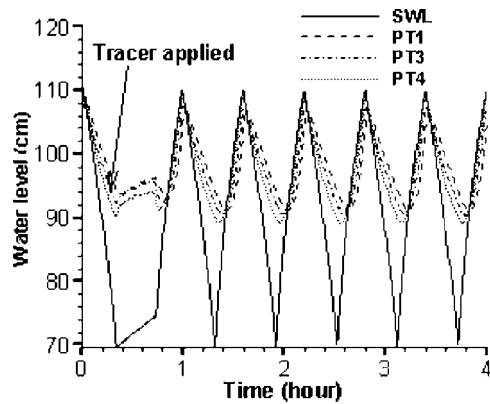


Fig. 8. Variation of the water table in the beach with tide (with and without waves). The lagging of the beach behind falling tides results in a persistent seaward hydraulic gradient. The injection of solution occurred at $t=22$ min and lasted approximately 20 min.

Waves Superimposed on Tide

In these experiments, the tide was varied between the elevations 70 and 110 cm in a tidal period of 37.5 min. The experiments started by subjecting the beach to at least two tidal cycles, and then stopping the tidal cycle at low tide. A 100 L of a NaCl solution at the concentration of 2.76 g/L was applied onto the beach within 16 min at the location $x=126$ cm, and the tidal cycle was continued. For experiments with waves, the wavemaker was started when the tide was present (i.e., waves were stopped only during tracer application). Two wave periods were selected: $T=1.0$ s and $T=1.25$ s. Two no-wave experiments were conducted and gave essentially the same result (Boufadel 1998). These were further analyzed in Boufadel et al. (2006), who explained the motion of the applied plume due to tide. They found that the applied plume moves seaward and downward. The seaward motion occurs during falling tides, and the downward motion occurs during rising tides. The latter is due to the fact that the tide fills the beach from above and not horizontally as hypothesized when using depth-averaged formulations, such as presented by Philip (1973) or Nielsen (1990). These works were seminal in terms of the movement of the beach water table, but they do not explain the two-dimensional motion in the beach. Further discussion on the two-dimensional motion in the beach can be found in Boufadel (2000).

When waves were present along with tide, considerable sand transport took place. Previous experiments showed that a steady-state sand profile was very hard to reach, and that the achievable equilibrium is a dynamic one, whereby the sand moves depending on the tide.

Fig. 8 reports the variation of the water levels with time starting from the high tide prior to application. As the tide level dropped, the most seaward transmitter (PT4) responded first, followed by PT3 and PT1. (PT2 was not functioning correctly). The water level in the beach rose during the tracer application, with the level at PT1 essentially equal to that of PT3. In the following times, one can clearly note the delayed response of the beach during the falling tides. This indicates that a seaward gradient exists in the beach, except near the high tide. Further discussion on the laboratory beach hydraulics during and after the tracer application is reported in Boufadel et al. (1998), wherein a numerical model that accounts for vadose zone hydraulics was used also.

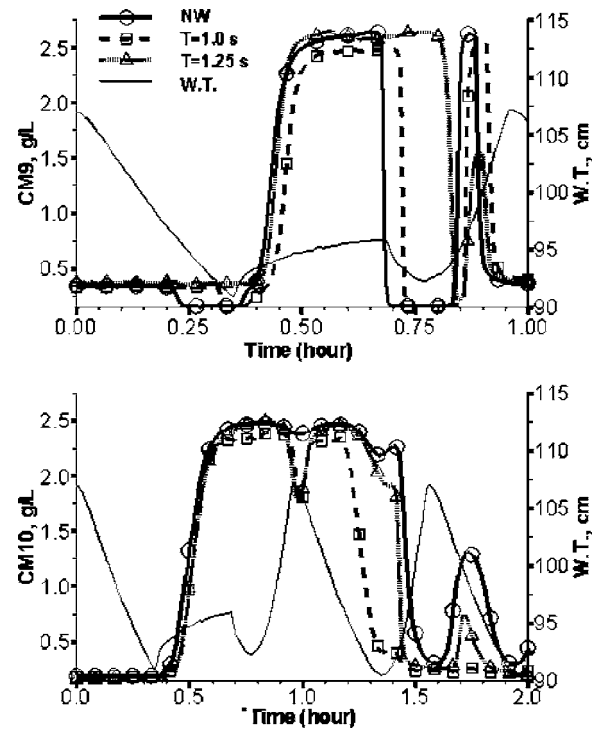


Fig. 9. Washout of the tracer from the top portion of the beach in the presence of tide. The right scale represents the water table (WT) elevation at PT3 (Fig. 1 and Table 1). Note the rise of the water level at $t=22$ min.

Figs. 9–11 report the variation of the concentration in the beach for the three cases (no wave, $T=1.0$ s and $T=1.25$ s). The sensors should give the same readings until the end of the tracer application, which is actually noted in Figs. 9–11 with some differences due to measurement errors. At CM9 [Fig. 9(a)], the concentration of the no-wave and $T=1.0$ s cases seem to give close results. This is probably because the runup for $T=1.0$ s waves was too small (15 cm) to affect the readings at CM9 when the SWL is below 95 cm. The long waves ($T=1.25$ s) appeared to have created a landward gradient that opposed the predominant seaward gradient due to the tide. This is because the breakthrough curve for $T=1.25$ s was about 20% wider than for the two other cases. Immediately after the tracer application, the concentration at CM9 dropped to zero for NW and $T=1.0$ s, because the sensor was exposed to the air (i.e., not submerged). Note that the sensor gives a reading of 0.15 g/L when submerged with tap water. The relatively large runup for the $T=1.25$ s case kept the sensor submerged, allowing it to give the high reading until it dropped for a short time at $t=0.8$ h. It rose again upon arrival of the high tide, but it was less than the NW and $T=1.0$ s cases. At times greater than 1.0 h, the concentration at CM9 rose to 0.15 g/L when the sensor was submerged and dropped to 0.0 g/L otherwise.

The concentration at CM10 [Fig. 9(b)] rose with the tracer application reaching the maximum value. It remained high for the NW case until the second tidal cycle, while it dropped by 20% for the wave cases near the first high tide. This indicates higher washout (lower residence time) due to waves from this section of the beach. For the case $T=1.0$ s, the concentration dropped during a falling tide (around $t=1.25$ h) and remained at the background value for the remainder of the experiment. During the rise of the second tide ($t=1.4$ h), the concentration for the NW and $T=1.25$ s behaved closely, but in the increase in concentration for

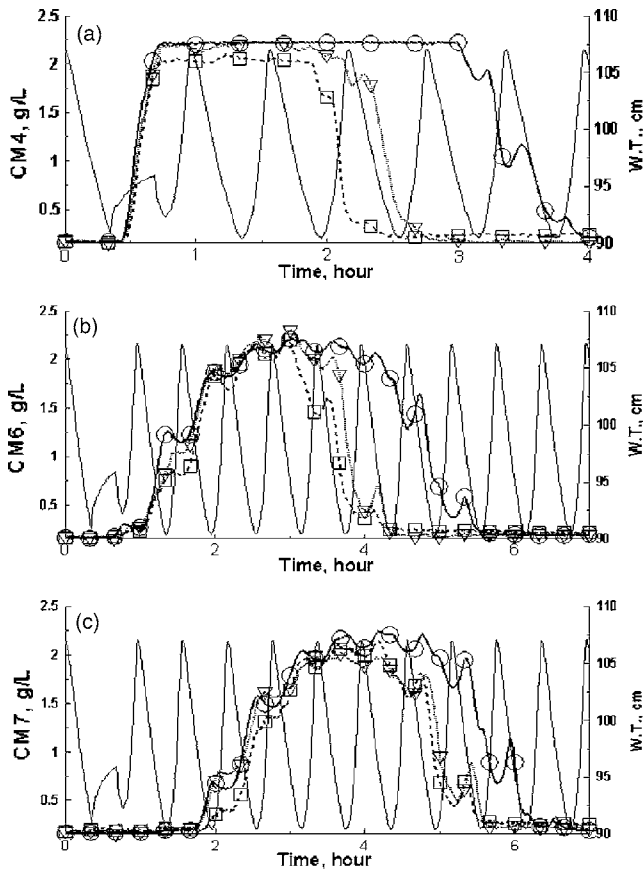


Fig. 10. Washout of the tracer from the middle portion of the beach in the presence of tide. The right scale represents the WT elevation at PT3 (Fig. 1 and Table 1).

$T=1.25$ s during the falling second tide ($t=1.75$ h) was only one-half of that of the no-wave case. This also indicates faster washout due to waves.

Fig. 10 shows the concentrations at CM4, CM6, and CM7, the sensors in the midsection of the beach. The rise of the concentration at CM4 seems independent of the beach hydrodynamics, most likely because the downward movement of the applied plume dominated the transport at that stage. The difference was apparent at other sensors, where the concentration for the no-wave case rose faster than the wave cases. The plume stayed longest at the sensors for the no-wave case followed by $T=1.25$ s and $T=1.0$ s. The difference between the wave cases was considerable for CM4, but smaller for other sensors, especially for CM7. The falling limbs of the breakthrough curves indicate that the concentration at these sensors decreased with the rising tides, which is due to the fact that the rising tide fills the beach (with water at the concentration of 0.15 g/L) almost vertically (Boufadel et al. 2006).

The readings at the sensors CM3 and CM5 provide indication on the downward movement of the plume. Figs. 11(a and b) show that waves increased the downward motion, causing the peaks to occur at about 60% of the peak of the no-wave case. The values for $T=1.0$ s case were relatively large, indicating a transport pathway that has less dilution than the other cases.

Fig. 11(c) provides the concentration variation at CM2, the most landward sensor. The rising part of the breakthrough curves indicates that the landward motion of the plume was largest for $T=1.25$ s followed by $T=1.0$ s and the no-wave case. Noting that

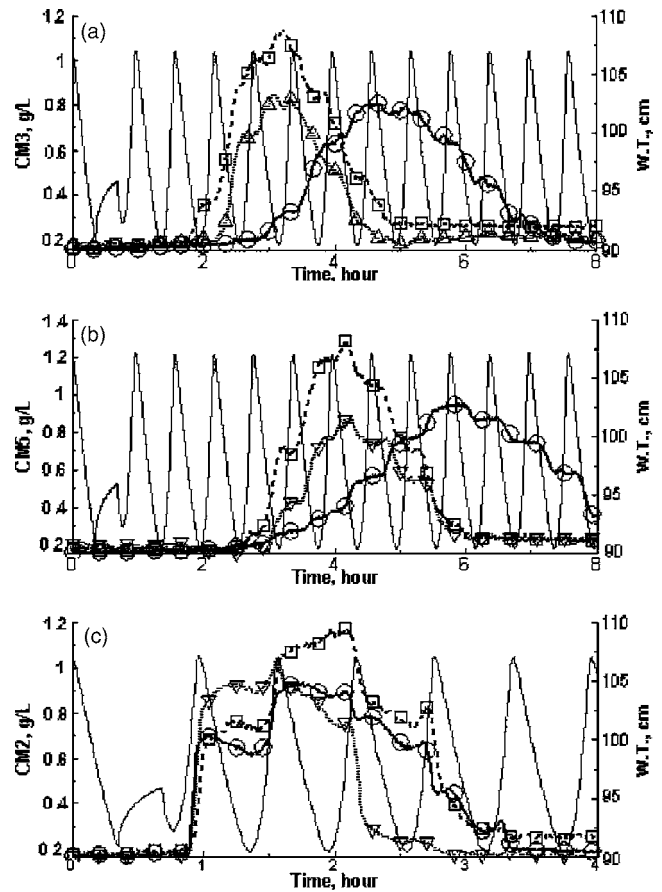


Fig. 11. Variation of the tracer with time in the lower (CM3 and CM5) and landward (CM2) portions of the beach. The right scale represents the WT elevation at PT3 (Fig. 1 and Table 1).

the runup of the $T=1.25$ s was larger than that of $T=1.0$ s, this indicates that the runup plays an important role in the transport of the plume landward of the high tide line (or in its proximity). This is unlike other sensors, such as CM4 and CM6 (Fig. 10) and CM3 and CM5 [Figs. 11(a and b)], where the increased washout resulted from waves with smaller runup (the $T=1.0$ s case). The maximum concentration in Fig. 11(c), however, is about 50% of the applied concentration, which is comparable to the deep sensors in the beach (CM3 and CM5). Noting the high value of concentration at CM9, the results in Fig. 11(c) indicate that the plume landward of the high tide line (or in proximity) was subjected to considerable dilution during its landward motion from CM9 to CM2.

An integral means to quantify the overall motion of the plume is “tracking” the variation of the centroid of the plume with time. Using the available sensors, the coordinates of the centroid of the plume are estimated by

$$X_G = \frac{M_{x,1}}{M_{x,0}} \quad (5a)$$

$$Z_G = \frac{M_{z,1}}{M_{z,0}} \quad (5b)$$

where M represents the spatial moment in the x or z direction, evaluated as

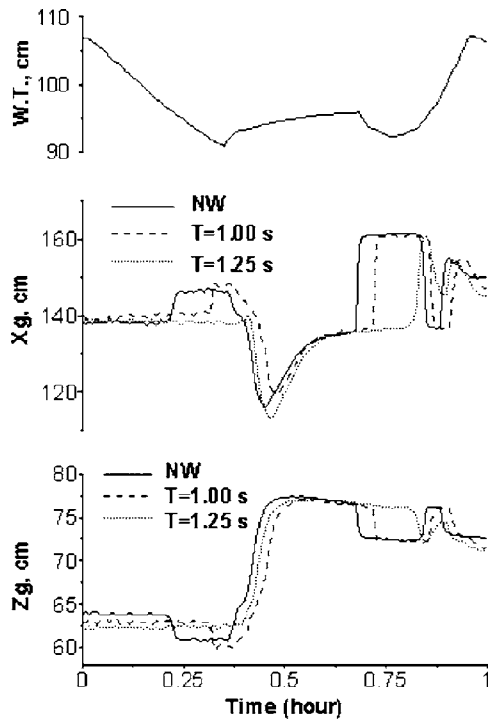


Fig. 12. Temporal variation of the coordinates of the plume centroid for time less than or equal to 1.0 h. The injection started at $t=22$ min and lasted for 20 min. An increase in X_G indicates seaward movement, while a decrease in Z_G indicates a downward movement. WT represents the water pressure at PT3.

$$M_{s,q} = \sum_{i=1}^{nc} s_i^q c_i \quad (6)$$

where $q=0$ or 1 , $s=x$ or z , c_i =concentration at the i th concentration sensor; and nc =total number of concentration sensors used to compute the moments. Although 10 sensors were used, the measurements of CM8 were always at the background level, and thus, were not used. For this reason, $nc=9$. Recall that the origin for the figure (i.e., $x=0$, $z=0$) is at the screen. Hence, an increase in X_G represents a seaward movement of the plume and a decrease in Z_G indicates a downward movement. Prior to the injection, the concentration in the tank was uniform (0.15 g/L). Upon substituting this uniform value in Eqs. (5) and (6) one obtains the coordinates of the centroid ($X_{Go} \approx 140$ cm, $Z_{Go} \approx 64$ cm). Boufadel et al. (2006) included the readings at CM8 and found 120 and 60 cm for the horizontal and vertical initial centroid positions, respectively. They erroneously stated that they have not used the readings at CM8.

Fig. 12 reports X_G , Z_G , and the water level at PT3 as function of time for the first hour of the experiment. During the injection, Z_G increased by about 20 cm, which is due to the introduced high concentrations in the upper part of the beach (CM9). The quantity X_G decreased initially because CM9 is more landward than X_{Go} , and it was the one of the first two CMs to respond to the injection of the solution (Fig. 9). X_G started increasing about 6.0 min after the beginning of injection, because the concentration at CM10, which is seaward of X_{Go} , increased. Immediately after the end of injection, a sudden increase in X_G is noted. It is because the water level dropped below the elevation of CM9, a landward sensor, causing this sensor to give a zero reading. Hence, the centroid shifted seaward. The effect of submersion (or its lack) on CM9

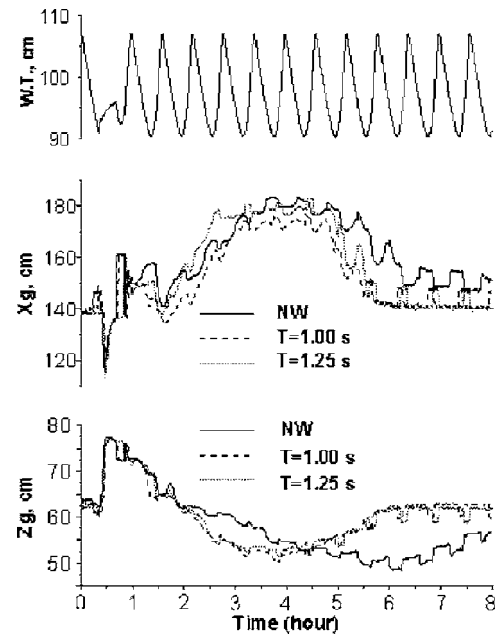


Fig. 13. Variation of the coordinates of the plume centroid as function of time for the duration of the experiment. Overall, waves accelerated the washout of tracer.

becomes negligible after $t=1.0$ h. Fig. 12(b) shows that waves delayed the seaward motion of the plume. The delay increased with the wave period. Fig. 12(c) shows that waves caused Z_G to stay longer at its high value at $t \approx 0.75$ h, which is probably because runup (especially of the long waves) caused the high concentration to stay longer at CM9 [Fig. 9(a)].

Between $t=2$ h and $t=4$ h, the rise of X_G [Fig. 13(b)] due to waves did not follow a clear pattern; it was slower than the no-wave case when $T=1.0$ s and faster when $T=1.25$ s. The plume, however, moved downward faster due to waves during this duration, as can be noted in Fig. 13(c). However, no clear difference existed between the wave cases in this figure. From $t=4$ h onward, the effects of waves became much clearer. Fig. 13(b) indicates that, when waves were present, X_G returned to its original value at $t \approx 6$ h, while it was still higher than the initial value at $t=8$ h for the no-wave case. Fig. 13(c) shows a fast increase of Z_G when waves are present. These findings indicate that the wave cases caused a faster washout of the tracer from the beach (to be accurate, the area encompassed by the conductivity meters).

If one estimates the residence time of the plume as the time at which the centroid locations return to their initial values, one concludes from Figs. 13(b and c) that the residence time of the plume subjected to waves superimposed on the tide is 75% ($6/8$ h) of that due to the tide only.

Discussion

This work investigated the washout of dissolved nutrients from a laboratory beach due to waves by conducting tracer studies in a laboratory beach facility (Fig. 1). The effects of the waves were studied in the case where the beach was subjected to the tide and that in which no tidal action was present. The following conclusions may be inferred.

1. Waves create a steep seaward hydraulic gradient in the swash zone and a mild seaward gradient landward of it

(Figs. 4 and 5). This has important implications for modeling solute transport to sea. Most studies use the difference in elevation between the landward water table and the mean sea level to compute the hydraulic gradient. Such an approach, results in an overestimation of the washout of the solutes to sea, because it ignores the presence of the mild gradient. In other words, taking the average gradient by ignoring the two zones is not accurate, because if ultimately the mild gradient is zero, the plume is not moving, no matter how steep the seaward gradient is in the swash zone.

2. Waves increased the residence time of a plume if they break seaward of it (Figs. 6 and 7). They also created pathways that are different from the ones that exist in the absence of waves. This was noted most clearly at CM7, where the concentration reached high values for the wave case [Fig. 7(b)], while it remained at the background value in the absence of waves [Fig. 6(b)].
3. In the presence of a tide that completely covered the solute plume, the waves increased the washout of the tracer from the intertidal zone of the beach in comparison with the no-wave case (see especially Figs. 10, 12, and 13). The residence time of the tracer plume due to the waves superimposed on the tide was estimated as 75% of that resulting from the tide with no waves. The effect of the waves was not uniform because they increased the residence time at CM9 (Fig. 9), which is near the beach surface. Based on the second conclusion above, it is hypothesized that if the plume is landward of the high tide line, its seaward transport is slower when waves are present, until it reaches the swash zone.

The tracer application strategy was adequate because the hydraulics of the system appears to be independent of the application period. The concentration of the solution (2.76 g/L) was too small to cause sinking of the plume due to negative buoyancy. This is an issue that was addressed in Boufadel (2000), and discussed thoroughly in Boufadel et al. (2006) (in their Discussion section).

Scaling up

There is an interest in scaling up the results of this study to natural sea conditions. In the coastal engineering literature, scaling up of waves setup using deep wave conditions and the slope of the beach has been a centerpiece. A good review is provided by Gourlay (1992). However, we are not aware of works that consider explicitly the dynamics of the water motion in porous media, well represented by Darcy's law (Freeze and Cherry 1979). This is rather unfortunate because we have developed, in a series of works, (Boufadel et al. 1998, 1999; Boufadel 2000) a dimensionless formulation for scaling up (or down) water flow and solute transport in variably-saturated media (i.e., below and above the water table). The formulation was used to scale up solute transport in the tank (Fig. 1) due to tides. However, we are not certain at this stage how to scale up the transport of solute in the beach due to waves. In other words, we are not sure to which wave length, height, or runup the results of this study correspond to if, for example, the whole domain is scaled up a factor of two. Thus, rigorous scaling up of waves from both groundwater and sea points of view is an unresolved issue at this stage.

Bioremediation

One of the main motivations of this study was for dealing with oil spills on beaches. A viable remediation technology is bioremedia-

tion which consists of stimulating the growth of hydrocarbon-degrading bacteria by amendment of nutrients, such as nitrate and phosphate (if they are at too low concentrations) (Venosa et al. 1996). An important goal of bioremediation of oil spills on beaches is ensuring the presence of sufficient amounts of nutrients in the intertidal zone at low tide. One of the method of nutrients application was used by Venosa et al. (1996), and consists of applying the nutrients to the bioremediation zone via a sprinkler system that would cover the whole intertidal zone. The application on the tidally-influenced beach in this study is less labor-intensive, and demonstrates that it suffices to apply the nutrients at one location near the high tide line to deliver high concentrations of nutrients near the beach surface; the concentration at CM9 and CM10 (Fig. 10) remained high prior to rising of the first tide. Although it cannot be ascertained in this study, but we believe that increasing the volume of solution would have caused the tracer to reach CM11. This is left for future study.

Acknowledgments

This work was supported, in part, by the U.S. Environmental Protection Agency's National Risk Management Research Laboratory, Cincinnati, Ohio under Cooperative Agreement No. CR-821029. However, it does not necessarily reflect the views of the Agency, and no official endorsement should be inferred.

Notation

The following symbols are used in this paper:

- C = wave propagation speed [LT^{-1}] [$C=L/T=gT/(2\pi)$];
- g = the gravity acceleration [LT^{-2}];
- H = wave height [L] (the vertical distance between crest and trough);
- h = water depth [L] (the average vertical distance of the wave crest and trough to the bottom);
- L = wave length [L] (the distance between two consecutive crests or troughs);
- T = the wave period [T] ($L=g/2\pi T^2$);
- X_G = horizontal coordinates [L] of the plume centroid estimated using the available sensors [Eqs. (5) and (6)];
- x = the horizontal distance [L] from the screen (positive seaward);
- y = the horizontal depth [L] from the plexiglass wall (positive inward perpendicular to the plan of Fig. 2);
- Z_G = vertical coordinates [L] of the plume centroid estimated using the available sensors [Eqs. (5) and (6)].
- z = the elevation [L] from the bottom of the tank; and

References

- Asservatham, A. M., Kang, H. Y., and Nielsen, P. (1993). "Groundwater movement in beach watertables." *Proc., 11th Australasian Conf. on Coastal and Ocean Engineering IE Aust.*, Crows Nest, NSW, Australia, Vol. 2, 589–594.
- Bear, J. (1988). *Dynamics of flow in porous media*, Dover, New York.
- Boufadel, M. C. (1998). "The transport of nutrients in beaches: Effect of tides, waves, and buoyancy." Ph.D. dissertation, Dept. of Civil and Environmental Engineering, Univ. of Cincinnati, Ohio.
- Boufadel, M. C. (2000). "A mechanistic study of nonlinear solute transport in a groundwater-surface water system under steady state and

- transient hydraulic conditions." *Water Resour. Res.*, 36, 2549–2565.
- Boufadel, M. C., Suidan, M. T., Rauch, C. H., Venosa, A. D., and Biswas, P. (1998). "2D variably saturated flows: Physical scaling and Bayesian estimation." *J. Hydrol. Eng.*, 3(4), 223–231.
- Boufadel, M. C., Suidan, M. T., and Venosa, A. D. (1999). "A numerical model for density-and-viscosity-dependent flow in two-dimensional variably-saturated media." *J. Contam. Hydrol.*, 37, 1–20.
- Boufadel, M. C., Suidan, M. T., and Venosa, A. D. (2006). "Tracer studies in laboratory beach simulating tidal influences." *J. Environ. Eng.*, 132(6), 616–623.
- Dean, R. G., and Dalrymple, R. A. (1984). *Water wave mechanics for engineers and scientists*, Prentice-Hall, New Jersey.
- Freeze, R. A., and Cherry, J. A. (1979). *Groundwater*, Prentice-Hall, Englewood Cliffs, N.J.
- Gourlay, M. R. (1992). "Wave set-up, wave run-up, and beach water table: Interaction between surf zone hydraulics and groundwater hydraulics." *Coastal Eng.*, 17, 93–144.
- Hegge, G. J., and Masselink, G. (1991). "Groundwater-table responses to wave run-up: An experimental study from Western Australia." *J. Coastal Res.*, 7, 623–634.
- Ippen, A. T. (1966). *Estuary and coastline hydrodynamics*, McGraw-Hill, New York.
- Longuet-Higgins, M. S., and Stewart, R. W. (1964). "Radiation stresses in water waves; a physical discussion with applications." *Deep-Sea Res.*, 11, 529–572.
- Melville, W. K., Veron, F., and White, C. J. (2002). "The velocity field under breaking waves: Coherent structures and turbulence." *J. Fluid Mech.*, 454, 203–233.
- Nielsen, P. (1989). "Measurements of wave setup and the coastal water table." *Proc., 9th Australasian Conf. on Coastal and Ocean Engineering*, Adelaide, 275–279.
- Nielsen, P. (1990). "Tidal dynamics of the water table in beaches." *Water Resour. Res.*, 26, 2127–2134.
- Philip, J. R. (1973). "Periodic nonlinear diffusion: An integral relation and its physical consequences." *Aust. J. Phys.*, 26, 513–519.
- Riedl, R. J., Huang, N., and Machan, R. (1972). "The subtidal pump: A mechanism of interstitial water exchange by water action." *Mar. Biol. (Berlin)*, 13, 210–221.
- Riedl, R. J., and Machan, R. (1972). "Hydrodynamic patterns in lotic intertidal sands and their bioclimatological implications." *Mar. Biol. (Berlin)*, 13, 179–209.
- Spielvogel, L. (1975). "Single-wave-runup on sloping beaches." *J. Fluid Mech.*, 74, 685–694.
- Svendsen, I. A. (1985). "Physical modelling of water waves." *Physical modelling in coastal engineering*.
- Venosa, A. D., et al. (1996). "Bioremediation of an experimental oil spill on the shoreline of Delaware Bay." *Environ. Sci. Technol.*, 30, 1764–1775.